Surprising Charge-Radius Kink in the Sc Isotopes at $N = 20$

Kristian König[1,2,*] Stephan Fritzsche[3,4] Gaute Hagen[5,6] Jason D. Holt[7,8] Andrew Klose[9] Jeremy Lantis[1,10]
Yuan Liu[1] Kei Minamisono[1,11,†] Takayuki Miyagi[2,12,13] Witold Nazarewicz[1,11] Thomas Papenbrock[6,14]
Skyy V. Pineda[1,10] Robert Powel[1,11] and Paul-Gerhard Reinhard[15]

[1]Facility for Rare Isotope Beams, Michigan State University, East Lansing, Michigan 48824, USA
[2]Department of Nuclear Physics, Technische Universität Darmstadt, 64289 Darmstadt, Germany
[3]Helmholtz Institute Jena, 07743 Jena, Germany
[4]Theoretisch-Physikalisches Institut, Friedrich-Schiller-Universität Jena, 07743 Jena, Germany
[5]Oak Ridge National Laboratory, Oak Ridge, Tennessee 37830, USA
[6]Department of Physics and Astronomy, University of Tennessee, Knoxville, Tennessee 37996, USA
[7]TRIUMF, Vancouver, British Colombia, V6T 2A3, Canada
[8]Department of Physics, McGill University, Montréal, Quebec, H3A 2T8, Canada
[9]Department of Chemistry and Biochemistry, Augustana University, Sioux Falls, South Dakota 57197, USA
[10]Department of Chemistry, Michigan State University, East Lansing, Michigan 48824, USA
[11]Department of Physics and Astronomy, Michigan State University, East Lansing, Michigan 48824, USA
[12]ExtreMe Matter Institute EMMI, GSI Helmholtzzentrum für Schwerionenforschung GmbH, 64291 Darmstadt, Germany
[13]Max-Planck-Institut für Kernphysik, Saupfercheckweg 1, 69117 Heidelberg, Germany
[14]Physics Division, Oak Ridge National Laboratory, Oak Ridge, Tennessee 37831, USA
[15]Friedrich-Alexander Universität, Erlangen 91058, Germany

Charge radii of neutron deficient ^{40}Sc and ^{41}Sc nuclei were determined using collinear laser spectroscopy. With the new data, the chain of Sc charge radii extends below the neutron magic number $N = 20$ and shows a pronounced kink, generally taken as a signature of a shell closure, but one notably absent in the neighboring Ca, K, and Ar isotopic chains. Theoretical models that explain the trend at $N = 20$ for the Ca isotopes cannot reproduce this puzzling behavior.

Introduction.—The introduction of the nuclear shell model [1,2] enabled the understanding of diverse observables, such as nuclear global properties and excitation energies. The numbers of nucleons that completely fill a shell are known as magic numbers, which are 2, 8, 20, 28, 50, 82, and 126 in stable nuclei. The simple structure of magic nuclei facilitates comparison with theories. With the advent of radioactive beam facilities, short-lived nuclei far from stability can be investigated, in which new magic numbers are found and the traditional shell closures vanish [3]. Particularly, the Ca isotopic chain at the proton-shell closure $Z = 20$ has been of great interest for nuclear structure studies since it features two stable doubly magic isotopes ^{40,48}Ca. The intricate pattern of charge radii along the Ca chain [4–8] has been a long-standing challenge for many-body nuclear theory; see discussion in, e.g., Refs. [6,8,9].

One interesting feature around magic gaps is a discontinuity, or a kink, in charge radii along isotopic or isotonic chains [10,11]. A number of theoretical models have been proposed to explain the kink, including pairing correlations, particle-vibrational coupling and ground-state-vibrational correlations, and spin-orbit effects [12–14]. The relation between the robustness of the magic number and the magnitude of the kink, however, is not obvious. In the Ca chain at $N = 28$, there is a prominent kink whose magnitude is comparable with that of the doubly magic ^{56}Ni [15], which is known to be a soft doubly magic nucleus [16] prone to polarization effects.

There is one exception at the magic number $N = 20$ for the Ca isotopic chain [7,8], where only a smooth variation of charge radii has been observed. The absence of a kink extends to the neighboring Ar [17] and K [18–20] chains. The origin of the apparent disappearance of kinks in the Ar, K, and Ca chains is still an open question. To shed light on this unusual behavior, we carried out a measurement of the charge radii across the $N = 20$ shell closure for the neutron-deficient Sc isotopes with $Z = 21$. At low energies, the Sc nuclei have an additional proton in the $0f_{7/2}$ shell outside the magic Ca core. The presence of the odd proton strongly impacts the core polarization, as evidenced by strong shape coexistence effects in the stable ^{45}Sc isotope [21]. The single proton in the $0f_{7/2}$ shell in ^{45}Sc may couple to the spherical ^{44}Ca core. On the other hand, a proton hole in the $0d_{3/2}$ shell weakly couples to the deformed ^{46}Ti core and leads to a collective behavior.

Since ^{40}Sc lies at the proton drip line [22], continuum effects may impact the charge radius [8], though due to the blocking effect of the unpaired neutron and proton in the $0d_{3/2}$ and $0f_{7/2}$ shell, respectively, the pairing effects are expected to be suppressed.

Experiment.—The ^{40,41}Sc isotopes were produced at the National Superconducting Cyclotron Laboratory by nucleon pickup of a ^{40}Ca primary beam at 140 MeV/nucleon in a Be target. The ions were separated using the A1900 fragment separator [23] and transported to a gas stopper [24], where the fast beam was thermalized. At a beam energy of 30 keV, the singly charged bare ions were transported to the BECOLA facility [25,26] with rates of approximately 15 000 and 20 000 ions/s for ^{40}Sc$^+$ and ^{41}Sc$^+$, respectively. There, the ions were guided into a helium-gas filled radio-frequency quadrupole trap (RFQ) [27], where they were cooled, accumulated, and extracted as ion bunches to reduce the laser background [28]. The ion beam was overlapped with a collinear laser beam using a 30° electrostatic deflector. Between two 3 mm apertures placed 2.1 m apart, photons were counted with photomultiplier tubes that were installed on top of a mirror-based detection system [25,29]. This detection region was floated on a scanning potential to perform Doppler tuning, which allowed us to operate the laser at a constant frequency while varying this potential by 250 V. To reference the isotope shift and to monitor potential long-term drifts, stable ^{45}Sc$^+$ was introduced into the BECOLA RFQ from an off-line Penning-ionization-gauge source [30] and probed every 4–6 h. When switching between the isotopes, the beam energy was kept constant and the laser frequency was adapted to match the different Doppler shift.

The $3p^63d4s\,^3D_2 \rightarrow 3p^63d4p\,^3F_3$ at 363.2 nm transition was investigated in ^{40,41,45}Sc$^+$. The employed continuous-wave Ti-sapphire laser (Matisse TS, Sirah Lasertechnik) was stabilized to a wavelength meter (WSU30, High-Finesse) and operated at 726 nm. The light was frequency doubled (Wavetrain, Spectra Physics) to 363 nm, transported via optical fiber to the beamline and irradiated in collinear geometry. Spectroscopy was performed with a laser power of 300 μW and a laser-beam diameter of 1 mm.

Results.—The obtained spectra are shown in Fig. 1. The lower signal quality of the ^{40}Sc$^+$ resonance spectrum is caused by a significant contamination with ^{40}Ar$^+$ from the gas stopping cell. Its rate exceeded the ^{40}Sc$^+$ rate by 3 orders of magnitude. To avoid overfilling the BECOLA RFQ, a short accumulation time of $t_{acc}(^{40}$Sc$^+) = 20$ ms had to be chosen, leading to a less efficient background suppression compared to ^{41}Sc$^+$ with $t_{acc}(^{41}$Sc$^+) = 1$ s.

The deduced isotope shifts $\delta\nu^{A,45} = \nu^A - \nu^{45}$ are listed in Table I together with literature values of other Sc isotopes. The statistical uncertainty was 1.7 and 6.8 MHz for ^{41}Sc$^+$ and ^{40}Sc$^+$, respectively, and approximately 1.1 MHz for the ^{45}Sc$^+$ reference spectra. The kinetic beam energy was determined with 10^{-5} relative accuracy by evaluating the
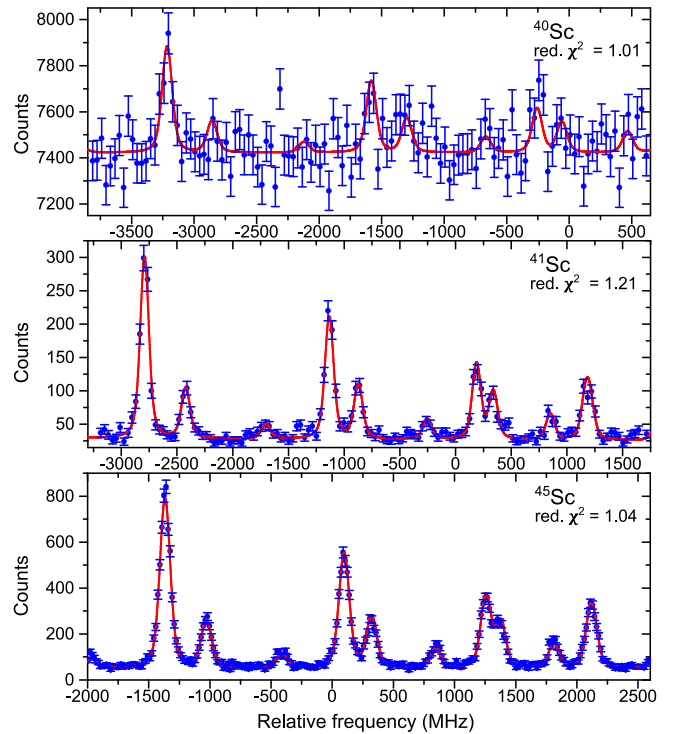

FIG. 1. Resonance spectra of the $3p^63d4s\,^3D_2 \rightarrow 3p^63d4p\,^3F_3$ transition in ^{40,41,45}Sc. The frequency is relative to the transition center of gravity of ^{45}Sc.

^{45}Sc$^+$ resonance frequencies together with its rest-frame frequency, which was measured via collinear and anticollinear spectroscopy beforehand as described in Ref. [31], leading to a 0.2 MHz uncertainty contribution.

To consider a varying filling rate of the buncher due to different purity of the ion beam, a general 2 MHz uncertainty is included, which corresponds to observations from stable beam measurements at BECOLA [32]. The laser frequency measurement was realized with a wavelength meter. According to a detailed study on devices from the same manufacturer [36,37] that we confirmed for our device [32], a 2.8 MHz contribution was considered. Because of the poor signal-to-noise ratio, the ^{40}Sc$^+$ spectrum could not be fitted without constraints and the ratios of the A and B parameters between the upper and lower level were fixed to those of ^{45}Sc$^+$. Nevertheless, the uncertainty of the B parameter was large and differed by 1.2σ from the theoretically expected value $[B_{lower}(\exp.) = 58(64)$ MHz, $B_{lower}(\text{theo.}) = -19$ MHz]; see Ref. [38] for a detailed study of the hyperfine splitting. Fixing the B parameter to the theoretical value leads to a shift of the center frequency by 2.3 MHz, which we consider as additional uncertainty. Adding the described contributions in quadrature leads to a total uncertainty of 8.1 and 4.0 MHz for ^{40}Sc and ^{41}Sc, respectively.

Atomic computations.—To describe the electronic response of the charge radii, detailed computations need to be performed, not only for the level structure but also the

TABLE I. Isotope shifts $\delta\nu^{A,A'}$, differential mean square charge radii $\delta\langle r^2\rangle^{A,A'}$, and rms charge radii R_{ch}. The isotope shifts of $^{42-46}$Sc are from [33,34], but the nuclear charge radius was updated with the improved calculations of the atomic factors. The statistical and systematic uncertainty is given in parentheses. In the systematic uncertainty of R, the uncertainty of the reference isotope ^{45}Sc of 0.0025 fm [35] is included.

A, A'	$I^P(A)$	$\delta\nu^{A,A'}$ (MHz)	Reference	$\delta\langle r^2\rangle^{A,A'}$ (fm^2)	$R_{\mathrm{ch}}(^A$Sc) (fm)
40, 45	4^-	$-1594(8)$	This Letter	$-0.226(22)(175)$	3.514 (3) (25)
41, 45	$7/2^-$	$-1199(4)$	This Letter	$-0.305(10)(137)$	3.503 (1) (20)
42, 45	0^+	$-985(11)$	[33]	0.076 (31) (100)	3.557 (4) (14)
42m, 42	7^+	$+74(5)$	[34]	$-0.210(14)(7)$	3.527 (5) (14)
43, 45	$7/2^-$	$-631(5)$	[33]	0.019(14)(65)	3.549 (2) (10)
44, 45	2^+	$-287(4)$	[33]	$-0.051(11)(32)$	3.539 (2) (5)
44m, 44	6^+	$+25(4)$	[33]	$-0.071(11)(2)$	3.529 (2) (5)
45, 45	$7/2^-$	0	[35]	0	3.5459 (0) (25)
45m, 45	$3/2^+$	$-66(2)$	[33]	0.187 (6) (6)	3.572 (1) (3)
46, 45	4^+	336 (3)	[33]	$-0.124(9)(31)$	3.528 (1) (5)

isotope (and hyperfine) parameters. Here, we have applied the multiconfiguration Dirac-Hartree-Fock (MCDHF) method [39], based on different advanced models, to generate the state functions and the electronic mass-shift $K^{(\mathrm{MS})}$ and field-shift parameter $F^{(\mathrm{el})}$ for the standard parametrization of atomic isotope shifts. For light elements, such as Sc, the mass shift $K^{(\mathrm{MS})} = K^{(\mathrm{NMS})} + K^{(\mathrm{SMS})}$, with $K^{(\mathrm{NMS})}$ being the so-called "normal" and $K^{(\mathrm{SMS})}$ the "specific" mass-shift coefficient, is known as the most critical. Since these mass-shift parameters are very sensitive to electron-electron correlations, the active space method with sizable expansions and virtual—single, double, and partly triple—excitations into additional layers of correlation orbitals need generally to be applied for their computations. Despite the advances in atomic theory during recent years, the nearly degenerate $3d$, $4s$, and $4p$ shells require to open also the $3s$ and $3p$ shells for their core-core contributions. This has made accurate isotope-shift parameters for open $3d$-shell elements a great challenge until today.

Three series of computations have been performed during the past decade for the $3p^63d4s\,^3D_2 \to 3p^63d4p\,^3F_3$ transition, based on the MCDHF method. These series are based on the independent implementations of this method with the RATIP [40], GRASP [41,42], and JAC [43] codes and give rise to the isotope-shift parameters in Table II. The (numerical) uncertainties reflect the overall stability of the computations

TABLE II. Comparison of the total mass-shift $K^{(\mathrm{MS})}$ and field-shift $F^{(\mathrm{el})}$ parameters as obtained from three independent implementations and series of computations.

Series	$K^{(\mathrm{MS})}$ (GHz u)	$F^{(\mathrm{el})}$ (MHz/fm^2)
Ref. [33]	$+583 \pm 30$	-355 ± 50
Ref. [34]	$+625 \pm 60$	-349 ± 15
This Letter	$+633 \pm 40$	-358 ± 20
Weighted mean	$+604 \pm 22$	-352 ± 12

by using a separate optimization of the upper and lower levels. To ensure their balance in the calculations, all series were started from a frozen set of occupied (spectroscopic) orbitals. The shear size of the computations require one to apply the weighted-mean value and the standard deviation to extract the (total) mass-shift parameter. Although these practical arguments cannot exclude a systematic shift, for instance, due to the omission of relevant interaction and correlation contributions, the independent setup of the codes and computations reduces this risk considerably. In the analysis below, we use $K^{(\mathrm{MS})} = 604 \pm 22$ GHz u and $F^{(\mathrm{el})} = -352 \pm 12$ MHz/fm^2.

The resulting differential mean square charge radii $\delta\langle r^2\rangle^{A,45}$ relative to the stable ^{45}Sc as well as the root-mean-square (rms) charge radii R_{ch} are listed in Table I. Note that the updated mass- and field-shift parameters were also applied to the previous measurements [33,34], which led to consistent charge radii, but smaller uncertainties.

Discussion.—The measured rms charge radii of Sc isotopes are plotted in Fig. 2 as stars (this Letter) and circles (results from Refs. [33,34]). The error bars correspond to the experimental uncertainty, while the gray area shows the full uncertainty, which is dominated by the uncertainty of the calculated mass- and field-shift parameters. In ^{42,44,45}Sc, there are isomeric states [33,34], whose charge radii are also shown in Fig. 2. For $N \geq 22$, the ground-state charge radii exhibit a similar trend to what has been observed for the Ca and Ti chains. Significant differences, however, are seen in the neutron-deficient isotopes. In particular, the rms charge radius of ^{41}Sc is significantly below that of ^{42}Sc, and the charge radius of ^{40}Sc rises with respect to that for ^{41}Sc, resulting in a pronounced kink structure at $N = 20$. The relatively large systematic uncertainty due to the atomic calculations cannot inhibit the kink since the variation of atomic factors can only tilt the entire trend around the ^{45}Sc pivot point.
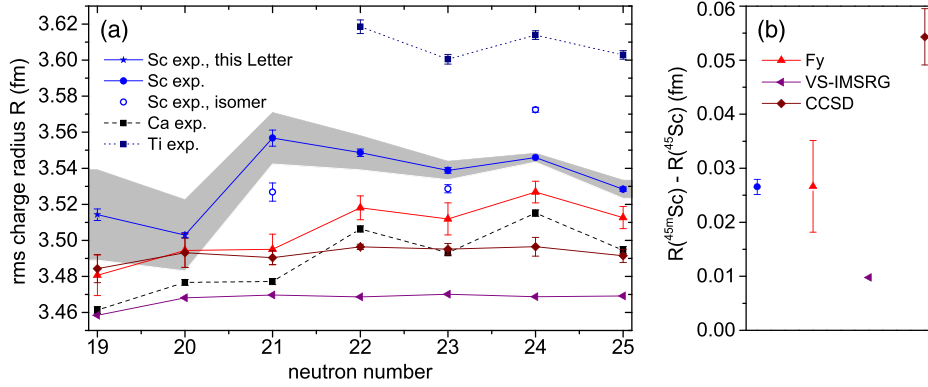
FIG. 2.   (a) Experimental and theoretical rms charge radii of Sc. The error bars indicate the experimental uncertainty, whereas the gray shaded area is the uncertainty that originates in the calculated mass- and field-shift factors. The atomic factors can cause a different tilt along the isotopic chain, but do not affect the overall trend, i.e., the appearance of a kink at $N = 20$. The experimental radii of isomeric Sc states [33,34] are plotted with open circles and, as a reference, the radii of the Ca [8] and Ti [44] isotopic chains are depicted. (b) Measured and calculated charge-radius difference between the $3/2^+$ isomeric state and the $7/2^-$ ground state of ^{45}Sc. When calculating the uncertainty of the Fy result, it was assumed that the calculated radii are not correlated; hence the corresponding error bar should be viewed as an upper limit [45].

The charge radii for the Sc isotopes were computed with the nuclear density functional (DFT), the coupled-cluster, and the valence-space in-medium similarity renormalization group (VS-IMSRG) theory. In DFT, we employed the Fayans functional within the full Hartree–Fock–Bogolyubov formalism, Fy(Δr, HFB) [8], that contains novel gradient terms in pairing and surface energies. Its parameters have been calibrated to the large dataset of ground-state properties in semimagic nuclei [46]. This model has been particularly successful in describing the neighboring Ca, K, and Ti isotopic chains [8,9,47]. The DFT calculations were done with the axial HFB solver, which allows for deformation and spin polarization. In order to compute the low-lying one- and two-quasiparticle excitations, we blocked all quasiparticle HFB states in the energy window of ± 6 MeV around the Fermi level. For even-N systems, we only blocked the proton quasiparticles, whereas for odd-N systems, we blocked both protons and neutrons. The resulting total energies were sorted energetically. All computed low-energy configurations turned out nearly spherical (within quadrupole deformation $|\beta_2| < 0.06$) and energies bunching approximately according to underlying spherical shells. As expected, the $0f_{7/2}$ shell corresponds to the lowest excitations for protons and for neutrons with $N > 20$. For $N = 19$, the $0d_{3/2}$ neutron shell yields the lowest energies. For even-N systems, the lowest configuration has $I^\pi = 7/2^-$ and we predict $I^\pi = 3/2^+$ isomers based on the $0d_{3/2} \rightarrow 0f_{7/2}$ proton excitation. These isomers are prolate-deformed with $\beta_2 \approx 0.25$, which agrees with the mean-field predictions of Ref. [21]. For odd-N isotopes, the situation is somehow ambiguous because we do not carry out the angular-momentum and isospin projection, which is essential when approaching $N \approx Z$ nuclei [48,49]. Thus, for given angular momentum I, we averaged

over all combinations with $I = I_p + I_n$. This average value is taken as an estimate of the angular momentum and the resulting variance serves as an estimate of the systematic error of the approximate projection. The second source of uncertainty is the statistical uncertainty, resulting from the parameter calibration. Calculations with broken spherical symmetry and broken time reversal symmetry result in changes of charge radii amounting to up to 0.01 fm.

The coupled-cluster and VS-IMSRG calculations employ the ΔNNLO$_{\rm GO}$(394) chiral nucleon-nucleon and three-nucleon interaction with explicit Delta isobars [50]. The coupled-cluster calculations [51–53] start from an axially symmetric Hartree-Fock reference state built from 13 spherical major oscillator shells with the oscillator frequency $\hbar\omega = 16$ MeV. The three-nucleon force had an additional energy cut of $E_{3\,\max} = 16\hbar\omega$. We consider two different types of Hartree-Fock reference states. The neutron(s) at the Fermi surface are in the $0f_{7/2}$ shell and fill pairs with $\pm j_z$, starting with $|j_z| = 1/2$; an odd neutron is then in the minimum positive j_z state. The proton in the $0f_{7/2}$ shell either has angular-momentum projection $j_z = 1/2$ or $j_z = 7/2$. The difference between both occupations is marked as an uncertainty. The former filling yields prolate deformations and the tentative spin-parity assignments are $I^\pi = 1/2^-, 1^+, 1/2^-, 2^+, 1/2^-, 3^+$ for ^{41,42,43,44,45}Sc, respectively, while the latter tentatively yields high spins and is more consistent with experiment. For ^{40}Sc, we have the odd neutron in the $0d_{3/2}$ shell with $j_z = 3/2$ and the spin-parity assignment is $I^\pi = 2^-$. Here, we assumed that $I = |I_z|$, as we did not perform the angular-momentum projection. For the $3/2^+$ isomer in ^{45}Sc, we had a proton hole on the $j_z = 3/2$ orbital of the $0d_{3/2}$ shell and two protons with $j_z = \pm 1/2$ in the $0f_{7/2}$ shell. The

coupled-cluster computations are performed in the singles and doubles approximation (CCSD). The point-proton radii are computed as an expectation value using the left and right ground state of the similarity transformed coupled-cluster Hamiltonian [54]. To obtain the charge radii, we include relativistic corrections and nucleon finite size effects [55].

The VS-IMSRG [56,57] is used to construct an approximate unitary transformation to decouple a multishell valence-space Hamiltonian [58] for proton-neutron $\{1s_{1/2}, 0d_{3/2}, 0f_{7/2}, 1p_{3/2}\}$ orbits above a ^{28}Si core, allowing for excitation across the $Z = N = 20$ shell gap. The VS-IMSRG decoupling is done within the 13 spherical major oscillator space with the frequency of 16 MeV. The $3N$ interaction matrix elements are included up to the sufficiently large truncation $E_{3\,\text{max}} = 24\hbar\omega$ [59]. The exact diagonalizations within the valence space are performed with the KSHELL code [60].

As illustrated in Fig. 2, the evolution of charge radii for $N \geq 22$ is well described by the Fy functional, which predicts a similar trend as in the Ca isotopes. The VS-IMSRG and CCSD calculations systematically underestimate the charge radii along the Sc chain. At the neutron-deficient side, all employed models are unable to explain the experimental trend below $N = 22$. In particular, they fail in reproducing the drastic decrease of charge radii between $N = 21$ and $N = 20$.

In the heavier odd-even system of ^{45}Sc, the charge-radius difference $\Delta R \equiv R(3/2^+) - R(7/2^-)$ between the deformed isomer and ground state, shown in Fig. 2(b), is correctly predicted by Fy, by taking into account quadrupole polarization effect of the proton $0d_{3/2} \rightarrow 0f_{7/2}$ excitation [21]. Indeed, the weak coupling of the proton hole in the $0d_{3/2}$ shell to the deformed ^{46}Ti core causes the increase of the radius, while the single proton in the $0f_{7/2}$ shell in ^{45}Sc couples to the spherical ^{44}Ca core [21]. As compared to experiment and Fy calculations, the VS-IMSRG approach significantly underestimates $\Delta R(^{45}\text{Sc})$, which is most likely due to its restricted configuration space, resulting in the underpredicted quadrupole collectivity [61]. In contrast, the CCSD approach, employing the axially deformed Hartree-Fock reference state, is capable of exploring larger collective spaces; this results in a fairly large value of ΔR and systematically larger values of charge radii along the Sc chain are predicted by this approach as compared to VS-IMSRG, see Fig. 2(a).

The positive parities and smaller radii of isomeric states in ^{42m}Sc and ^{44m}Sc suggest that these excitations involve $0f_{7/2}$ neutrons and $0f_{7/2}$ protons that do not lead to strong polarization effects. The low values of charge radii in ^{42m}Sc and ^{44m}Sc have not yet been explained [33,34]. It has to be stressed that the $T = 0$, $I = 0$ ground state of ^{42}Sc cannot be represented by a single mean-field configuration [48]. This suggests [49] that, when it comes to the DFT description of charge radii differences between the isovector and isoscalar configurations of ^{42}Sc and ^{44}Sc, a multireference approach involving angular-momentum and isospin projection is required.

Summary.—Charge radii of the neutron-deficient scandium isotopes ^{40}Sc and ^{41}Sc were determined using collinear laser spectroscopy. The new data demonstrate the presence of an appreciable kink structure at the $N = 20$ neutron-shell closure, which is absent in the neighboring Ca, K, and Ar isotopic chains.

The experimental data on charge radii were interpreted using *ab initio* and DFT models employing realistic interactions. All models are consistent with the data for $N \geq 22$, but fail in reproducing the experimental pattern in charge radii for neutron-deficient isotopes, including the kink structure at $N = 20$. At the same time, the employed models have been successful in explaining the absence of the kink in the Ca isotopic chain. We thus conclude that the charge-radius anomaly at ^{41}Sc poses a significant puzzle for nuclear theory. Additional measurements of charge radii in the Ti isotopic chain across $N = 20$ are called for, as well as further theoretical studies of core polarization effects in this mass region.

*kkoenig@ikp.tu-darmstadt.de
†minamiso@frib.msu.edu

[1] M. Goeppert-Mayer, On closed shells in nuclei. II, Phys. Rev. **75**, 1969 (1949).

[2] O. Haxel, J. H. D. Jensen, and H. E. Suess, On the "magic numbers" in nuclear structure, Phys. Rev. **75**, 1766 (1949).

[3] O. Sorlin and M.-G. Porquet, Nuclear magic numbers: New features far from stability, Prog. Part. Nucl. Phys. **61**, 602 (2008).

[4] A.-M. Mårtensson-Pendrill, A. Ynnerman, H. Warston, L. Vermeeren, R. E. Silverans, A. Klein, R. Neugart, C. Schulz, and P. Lievens (ISOLDE Collaboration), Isotope shifts and nuclear-charge radii in singly ionized $^{40-48}$Ca, Phys. Rev. A **45**, 4675 (1992).

[5] L. Vermeeren, R. E. Silverans, P. Lievens, A. Klein, R. Neugart, C. Schulz, and F. Buchinger, Ultrasensitive Radioactive Detection of Collinear-Laser Optical Pumping: Measurement of the Nuclear Charge Radius of ^{50}Ca, Phys. Rev. Lett. **68**, 1679 (1992).

[6] R. Garcia Ruiz et al., Unexpectedly large charge radii of neutron-rich calcium isotopes, Nat. Phys. **12**, 594 (2016).

[7] L. Vermeeren, P. Lievens, R. E. Silverans, U. Georg, M. Keim, A. Klein, R. Neugart, M. Neuroth, and F. Buchinger (ISOLDE Collaboration), The mean square nuclear charge radius of Ca-39, J. Phys. G **22**, 1517 (1996).

[8] A. Miller, K. Minamisono, A. Klose, D. Garand, C. Kujawa, J. Lantis, Y. Liu, B. Maaß, P. Mantica, W. Nazarewicz, W. Nörtershäuser, S. Pineda, P. Reinhard, D. Rossi, F. Sommer, C. Sumithrarachchi, A. Teigelhöfer, and J. Watkins, Proton superfluidity and charge radii in proton-rich calcium isotopes, Nat. Phys. **15**, 432 (2019).

[9] M. Kortelainen, Z. Sun, G. Hagen, W. Nazarewicz, T. Papenbrock, and P.-G. Reinhard, Universal trend of charge radii of even-even Ca–Zn nuclei, Phys. Rev. C **105**, L021303 (2022).

[10] E. W. Otten, Nuclear Radii and Moments of Unstable Isotopes, Treatise on Heavy Ion Science Vol. 8: Nuclei far from Stability [Plenum Publishing Corp. (Springer), New York, 1989].

[11] P. Campbell, I. Moore, and M. Pearson, Laser spectroscopy for nuclear structure physics, Prog. Part. Nucl. Phys. **86**, 127 (2016).

[12] C. Gorges et al., Laser Spectroscopy of Neutron-Rich Tin Isotopes: A Discontinuity in Charge Radii across the $N = 82$ Shell Closure, Phys. Rev. Lett. **122**, 192502 (2019).

[13] P.-G. Reinhard and W. Nazarewicz, Nuclear charge densities in spherical and deformed nuclei: Toward precise calculations of charge radii, Phys. Rev. C **103**, 054310 (2021).

[14] U. C. Perera, A. V. Afanasjev, and P. Ring, Charge radii in covariant density functional theory: A global view, Phys. Rev. C **104**, 064313 (2021).

[15] F. Sommer et al., Charge Radii of ^{55,56}Ni Reveal Surprisingly Similar Behavior at $N = 28$ in Ca and Ni Isotopes, Phys. Rev. Lett. **129**, 132501 (2022).

[16] T. Otsuka, M. Honma, and T. Mizusaki, Structure of the $N = Z = 28$ Closed Shell Studied by Monte Carlo Shell Model Calculation, Phys. Rev. Lett. **81**, 1588 (1998).

[17] A. Klein, B. Brown, U. Georg, M. Keim, P. Lievens, R. Neugart, M. Neuroth, R. Silverans, L. Vermeeren (ISOLDE Collaboration), Moments and mean square charge radii of short-lived argon isotopes, Nucl. Phys. **A607**, 1 (1996).

[18] F. Touchard, P. Guimbal, S. Büttgenbach, R. Klapisch, M. De Saint Simon, J. Serre, C. Thibault, H. Duong, P. Juncar, S. Liberman, J. Pinard, and J. Vialle, Isotope shifts and hyperfine structure of $^{38-47}$K by laser spectroscopy, Phys. Lett. **108B**, 169 (1982).

[19] J. A. Behr, A. Gorelov, T. Swanson, O. Häusser, K. P. Jackson, M. Trinczek, U. Giesen, J. M. D'Auria, R. Hardy, T. Wilson, P. Choboter, F. Leblond, L. Buchmann, M. Dombsky, C. D. P. Levy, G. Roy, B. A. Brown, and J. Dilling, Magneto-optic Trapping of β-Decaying ^{38}K^m, ^{37}K from an on-line Isotope Separator, Phys. Rev. Lett. **79**, 375 (1997).

[20] D. M. Rossi, K. Minamisono, H. B. Asberry, G. Bollen, B. A. Brown, K. Cooper, B. Isherwood, P. F. Mantica, A. Miller, D. J. Morrissey, R. Ringle, J. A. Rodriguez, C. A. Ryder, A. Smith, R. Strum, and C. Sumithrarachchi, Charge radii of neutron-deficient ^{36}K and ^{37}K, Phys. Rev. C **92**, 014305 (2015).

[21] P. Bednarczyk et al., High spin states in ^{45}Sc and coexistence of collective and non-collective structures in the odd-A $f_{7/2}$ nuclei, Phys. Lett. B **393**, 285 (1997).

[22] C. Woods, W. Catford, L. Fifield, and N. Orr, A measurement of the mass of ^{39}Sc, Nucl. Phys. **A484**, 145 (1988).

[23] D. Morrissey, B. Sherrill, M. Steiner, A. Stolz, and I. Wiedenhoever, Commissioning the A1900 projectile fragment separator, Nucl. Instrum. Methods Phys. Res., Sect. B **204**, 90 (2003).

[24] K. Cooper, C. Sumithrarachchi, D. Morrissey, A. Levand, J. Rodriguez, G. Savard, S. Schwarz, and B. Zabransky, Extraction of thermalized projectile fragments from a large volume gas cell, Nucl. Instrum. Methods Phys. Res., Sect. A **763**, 543 (2014).

[25] K. Minamisono, P. Mantica, A. Klose, S. Vinnikova, A. Schneider, B. Johnson, and B. Barquest, Commissioning of the collinear laser spectroscopy system in the BECOLA facility at NSCL, Nucl. Instrum. Methods Phys. Res., Sect. A **709**, 85 (2013).

[26] D. M. Rossi, K. Minamisono, B. R. Barquest, G. Bollen, K. Cooper, M. Davis, K. Hammerton, M. Hughes, P. F. Mantica, D. J. Morrissey, R. Ringle, J. A. Rodriguez, C. A. Ryder, S. Schwarz, R. Strum, C. Sumithrarachchi, D. Tarazona, and S. Zhao, A field programmable gate array-based time-resolved scaler for collinear laser spectroscopy with bunched radioactive potassium beams, Rev. Sci. Instrum. **85**, 093503 (2014).

[27] B. Barquest, G. Bollen, P. Mantica, K. Minamisono, R. Ringle, S. Schwarz, and C. Sumithrarachchi, RFQ beam cooler and buncher for collinear laser spectroscopy of rare isotopes, Nucl. Instrum. Methods Phys. Res., Sect. A **866**, 18 (2017).

[28] A. Nieminen, P. Campbell, J. Billowes, D. H. Forest, J. A. R. Griffith, J. Huikari, A. Jokinen, I. D. Moore, R. Moore, G. Tungate, and J. Äystö, On-Line Ion Cooling and Bunching for Collinear Laser Spectroscopy, Phys. Rev. Lett. **88**, 094801 (2002).

[29] B. Maaß, K. König, J. Krämer, A. Miller, K. Minamisono, W. Nörtershäuser, and F. Sommer, A 4π fluorescence detection region for collinear laser spectroscopy, arXiv:2007.02658.

[30] C. Ryder, K. Minamisono, H. Asberry, B. Isherwood, P. Mantica, A. Miller, D. Rossi, and R. Strum, Population distribution subsequent to charge exchange of 29.85 keV Ni^+ on sodium vapor, Spectrochim. Acta B Atom. Spectros. **113**, 16 (2015).

[31] K. König, K. Minamisono, J. Lantis, S. Pineda, and R. Powel, Beam energy determination via collinear laser spectroscopy, Phys. Rev. A **103**, 032806 (2021).

[32] K. König, F. Sommer, J. Lantis, K. Minamisono, W. Nörtershäuser, S. Pineda, and R. Powel, Isotope-shift measurements and king-fit analysis in nickel isotopes, Phys. Rev. C **103**, 054305 (2021).

[33] M. Avgoulea et al., Nuclear charge radii and electromagnetic moments of radioactive scandium isotopes and isomers, J. Phys. G **38**, 025104 (2011).

[34] A. Koszorús, L. Vormawah, R. Beerwerth, M. Bissell, P. Campbell, B. Cheal, C. Devlin, T. Eronen, S. Fritzsche, S. Geldhof, H. Heylen, J. Holt, A. Jokinen, S. Kelly, I. Moore, T. Miyagi, S. Rinta-Antila, A. Voss, and C. Wraith, Proton-neutron pairing correlations in the self-conjugate nucleus ^{42}Sc, Phys. Lett. B **819**, 136439 (2021).

[35] I. Angeli and K. Marinova, Table of experimental nuclear ground state charge radii: An update, At. Data Nucl. Data Tables **99**, 69 (2013).

[36] M. Verlinde, K. Dockx, S. Geldhof, K. König, D. Studer, T. Cocolios, R. de Groote, R. Ferrer, Y. Kudryavtsev, T. Kieck, I. Moore, W. Nörtershäuser, S. Raeder, P. Bergh, P. Van Duppen, and K. Wendt, On the performance of wavelength meters: Part 1—consequences for medium-to-high-resolution laser spectroscopy, Appl. Phys. B **126**, 85 (2020).

[37] K. König, P. Imgram, J. Krämer, B. Maaß, K. Mohr, T. Ratajczyk, F. Sommer, and W. Nörtershäuser, On the performance of wavelength meters: Part 2—frequency-comb based characterization for more accurate absolute wavelength determinations, Appl. Phys. B **126**, 86 (2020).

[38] R. Powel, B. A. Brown, J. D. Holt, A. Klose, K. König, J. Lantis, K. Minamisono, T. Miyagi, and S. Pineda, Ground state magnetic dipole moment of ^{40}Sc, Phys. Rev. C **105**, 034310 (2022).

[39] I. P. Grant, *Relativistic Quantum Theory of Atoms and Molecules: Theory and Computation* (Springer, Berlin, Heidelberg, Germany, 2007).

[40] S. Fritzsche, The RATIP program for relativistic calculations of atomic transition, ionization and recombination properties, Comput. Phys. Commun. **183**, 1525 (2012).

[41] P. Jönsson, G. Gaigalas, J. Bieroń, C. F. Fischer, and I. Grant, New version: GRASP2K relativistic atomic structure package, Comput. Phys. Commun. **184**, 2197 (2013).

[42] C. Nazé, E. Gaidamauskas, G. Gaigalas, M. Godefroid, and P. Jönsson, RIS3: A program for relativistic isotope shift calculations, Comput. Phys. Commun. **184**, 2187 (2013).

[43] S. Fritzsche, A fresh computational approach to atomic structures, processes and cascades, Comput. Phys. Commun. **240**, 1 (2019).

[44] Y. P. Gangrsky, K. P. Marinova, S. G. Zemlyanoi, I. D. Moore, J. Billowes, P. Campbell, K. T. Flanagan, D. H. Forest, J. A. R. Griffith, J. Huikari, R. Moore, A. Nieminen, H. Thayer, G. Tungate, and J. Äystö, Nuclear charge radii of neutron deficient titanium isotopes ^{44}Ti and ^{45}Ti, J. Phys. G **30**, 1089 (2004).

[45] P.-G. Reinhard and W. Nazarewicz, Statistical correlations of nuclear quadrupole deformations and charge radii, Phys. Rev. C **106**, 014303 (2022).

[46] P. Klüpfel, P.-G. Reinhard, T. J. Bürvenich, and J. A. Maruhn, Variations on a theme by Skyrme, Phys. Rev. C **79**, 034310 (2009).

[47] A. Koszorús et al., Charge radii of exotic potassium isotopes challenge nuclear theory and the magic character of $N = 32$, Nat. Phys. **17**, 439 (2021).

[48] W. Satuła, J. Dobaczewski, W. Nazarewicz, and T. R. Werner, Isospin-breaking corrections to superallowed fermi β decay in isospin- and angular-momentum-projected nuclear density functional theory, Phys. Rev. C **86**, 054316 (2012).

[49] W. Satuła and W. Nazarewicz, Isospin effects in $n \approx z$ nuclei in extended density functional theory, Phys. Scr. **91**, 023013 (2016).

[50] W. G. Jiang, A. Ekström, C. Forssén, G. Hagen, G. R. Jansen, and T. Papenbrock, Accurate bulk properties of nuclei from $a = 2$ to ∞ from potentials with Δ isobars, Phys. Rev. C **102**, 054301 (2020).

[51] H. Kümmel, K. H. Lührmann, and J. G. Zabolitzky, Many-fermion theory in expS- (or coupled cluster) form, Phys. Rep. **36**, 1 (1978).

[52] R. J. Bartlett and M. Musiał, Coupled-cluster theory in quantum chemistry, Rev. Mod. Phys. **79**, 291 (2007).

[53] G. Hagen, T. Papenbrock, M. Hjorth-Jensen, and D. J. Dean, Coupled-cluster computations of atomic nuclei, Rep. Prog. Phys. **77**, 096302 (2014).

[54] S. J. Novario, G. Hagen, G. R. Jansen, and T. Papenbrock, Charge radii of exotic neon and magnesium isotopes, Phys. Rev. C **102**, 051303(R) (2020).

[55] G. Hagen, A. Ekström, C. Forssén, G. R. Jansen, W. Nazarewicz, T. Papenbrock, K. A. Wendt, S. Bacca, N. Barnea, B. Carlsson, C. Drischler, K. Hebeler, M. Hjorth-Jensen, M. Miorelli, G. Orlandini, A. Schwenk, and J. Simonis, Neutron and weak-charge distributions of the ^{48}Ca nucleus, Nat. Phys. **12**, 186 (2016).

[56] S. R. Stroberg, A. Calci, H. Hergert, J. D. Holt, S. K. Bogner, R. Roth, and A. Schwenk, Nucleus-Dependent Valence-Space Approach to Nuclear Structure, Phys. Rev. Lett. **118**, 032502 (2017).

[57] S. R. Stroberg, H. Hergert, S. K. Bogner, and J. D. Holt, Nonempirical interactions for the nuclear shell model: An update, Annu. Rev. Nucl. Part. Sci. **69**, 307 (2019).

[58] T. Miyagi, S. R. Stroberg, J. D. Holt, and N. Shimizu, *Ab initio* multishell valence-space Hamiltonians and the island of inversion, Phys. Rev. C **102**, 034320 (2020).

[59] T. Miyagi, S. R. Stroberg, P. Navrátil, K. Hebeler, and J. D. Holt, Converged *ab initio* calculations of heavy nuclei, Phys. Rev. C **105**, 014302 (2022).

[60] N. Shimizu, T. Mizusaki, Y. Utsuno, and Y. Tsunoda, Thick-restart block Lanczos method for large-scale shell-model calculations, Comput. Phys. Commun. **244**, 372 (2019).

[61] S. R. Stroberg, J. Henderson, G. Hackman, P. Ruotsalainen, G. Hagen, and J. D. Holt, Systematics of $e2$ strength in the sd shell with the valence-space in-medium similarity renormalization group, Phys. Rev. C **105**, 034333 (2022).

[62] S. R. Stroberg, In-Medium Similarity Renormalization Group software for nuclear structure calculations, https://github.com/ragnarstroberg/imsrg.